Neuroscience Research xxx (xxxx) xxx

Contents lists available at ScienceDirect

Neuroscience Research

journal homepage: www.sciencedirect.com/journal/neuroscience-research

Nerve terminals in the tumor microenvironment as targets for local infiltration analgesia

Pallavi Madhusudanan [a], Chinnu Jerard [a], Gayathri Raju [a], Neeraj Katiyar [b], Sahadev A. Shankarappa [a,*]

[a] Amrita School of Nanosciences & Molecular Medicine, Amrita Institute of Medical Sciences & Research Center, Amrita Vishwa Vidyapeetham, Kochi, Kerala 682041, India

[b] Biomedical Engineering Division, Department of Materials Science and Engineering, Uppsala University, Lagerhyddsvagen 1, 752 37 Uppsala, Sweden

ARTICLE INFO

Keywords:
Cancer pain
Opioids
Hyperalgesia
Analgesia
Calcium channel
TRPV1
Innervation

ABSTRACT

Nerve terminals within the tumor microenvironment as potential pain-mitigating targets for local infiltration analgesia is relatively less explored. In this study, we examine the role of key analgesics administered as local infiltration analgesia in a model of cancer-induced bone pain (CIBP). CIBP was induced by administration of allogenic MRMT1 breast cancer cells in the proximal tibia of rats, and tumor mass characterized using radiogram, micro-CT, and histological analysis. In vitro responsiveness to key analgesics δ-opioid receptor agonist (DOPr), Ca^{2+} channel and TRPV1 antagonists was assessed using ratiometric Ca^{2+} imaging in sensory neurons innervating the tumor site. Effectiveness of locally infiltrated analgesics administered independently or in combination was assessed by quantifying evoked limb withdrawal thresholds at two distinct sites for up to 14 days. CIBP animals demonstrated DOPr, N-, and L-type and TRPV1 expression in lumbar dorsal root ganglion neurons (DRG), comparable to controls. Evoked Ca^{2+} transients in DRG neurons from CIBP animals were significantly reduced in response to treatment with compounds targeting DOPr, N-, L-type Ca^{2+} channels and TRPV1 proteins. Behaviourally, evoked hyperalgesia at the tumor site was strongly mitigated by peritumoral injection of the DOPr agonist and T-type calcium antagonist, via its activity on bone afferents. Results from this study suggest that nerve terminals at tumor site could be utilized as targets for specific analgesics, using local infiltration analgesia.

1. Introduction

Cancer pain is a debilitating condition that affects a large segment of patients diagnosed with cancer. The prevalence and burden of the disease is not completely known, but approximately two thirds of patients diagnosed with advanced cancer reportedly suffer from pain that needs active management (van den Beuken-van Everdingen et al., 2007). With advances in cancer treatment, people with cancer are living longer, and invariably enduring cancer associated pain for prolonged periods of time. Hence, strategies for robust pain management in cancer pain patients has become a necessity. Current therapeutical options such as radiotherapy, chemotherapy, analgesics, bisphosphonates, immunotherapy, and nerve blocks provide pain relief but, 30% of patients still report inadequate pain management (Vuong et al., 2016). Systemically administered opioids, non-steroidal anti-inflammatory drugs, and certain anti-convulsants have been commonly utilized with good results (Sliepen, 2021). Even though systemic analgesics provide excellent pain management, their short half-life, physical dependence, tolerance, and undesirable off-target effects make them difficult front-line agents for managing cancer pain (Benyamin et al., 2008). Alternate strategies need to be explored to supplement existing treatment modalities. One such strategy is the local application of analgesics around the vicinity of the tumor mass to modulate peripheral nociceptors within the tumor microenvironment.

It is well known that onset of cancer pain is dependent on the anatomical location and the histological type of the cancer lesion (Schmidt et al., 2010). In addition, tumor heterogeneity plays an important role in determining the tumor microenvironment milieu, which ultimately effects pain generation typical for the tumor type (Sabino et al., 2003; Colotta et al., 2009; Schmidt et al., 2010). Even though the exact etiology of cancer pain is not completely clear, it is widely believed that cancer cells secrete a variety of cytokines into the

* Correspondence to: Amrita School of Nanosciences and Molecular Medicine, Amrita Institute of Medical Sciences and Research Center, Amrita Vishwa Vidyapeetham University, Kochi, Kerala 682041, India.

E-mail addresses: sahadevs@icloud.com, sahadevs@aims.amrita.edu (S.A. Shankarappa).

https://doi.org/10.1016/j.neures.2023.06.006
Received 7 January 2023; Received in revised form 19 May 2023; Accepted 16 June 2023
Available online 17 June 2023

tumor microenvironment. The putative cytokine mediators bind and activate primary afferent nerve terminals within the tumor microenvironment, subsequently leading to the generation of pain signals (Zheng et al., 2022). In addition to tumor associated compression of nerve terminals, release of tumor cell- and inflammatory cell- derived pain-stimulatory molecules such as endothelin, prostaglandin E2 (PGE2), interleukins, nerve growth factor (NGF) and others, have been shown to sensitize nerve terminals located near the tumor (Dushyanthen et al., 2013). Further, presence of an inflammatory milieu within the tumor microenvironment has been shown to result in acute, and long-term enhancement of neuronal excitability (Khasabova et al., 2007), changes in synaptic plasticity, central sensitization (Urch et al., 2003) and heightened pain behavioral response (Falk and Dickenson, 2014). Systemic administration of various categories of analgesics including δ opioid receptor (DOPr) agonists, voltage-gated calcium channel inhibitors, transient receptor potential vanilloid 1(TRPV1) and transient receptor potential ankyrin 1 antagonists have shown good anti-nociceptive effect in animal models of cancer pain (Ghilardi et al., 2005; Niiyama et al., 2009; de Almeida et al., 2021). However, it is important to note that only few studies have explored the effects of local infiltration of analgesic agents around tumors in attenuating cancer pain (Menéndez et al., 2003; Baamonde et al., 2005). Drug delivery, especially in the form of prolonged release systems and infusion pumps for local infiltration analgesia may potentially be utilized for managing selective painful tumors.

In this study, we sought to examine the feasibility of locally targeting peripheral nerve terminals in the tumor vicinity as an alternative approach for administration of analgesic agents to mitigate cancer associated pain. To specifically explore local and referred cancer pain, we have utilized a murine model of cancer induced bone pain (CIBP). The rationale for using this model is the localized anatomical site of the induced tumor, rich peripheral nerve terminals, and site-specific nerve innervations that arise at identifiable spinal level ganglia. The goal of the study was to determine the extent of responsiveness of peripheral nerve terminals in the tumor vicinity to injectable analgesics. Using the CIBP model, we explore effects of three main category of analgesics, namely, peripheral opioid (DOPr) agonist, calcium (Ca^{2+}) channel antagonists (L-, N- and T-type) and TRP receptor antagonist (TRPV1). The analgesics were locally administered as peri-tumoral injections around tumor afflicted bone. We assessed whether these agents given independently or in combinations could reduce intra-neuronal calcium levels in cancer-sensitized sensory neurons and reverse bone-tumor induced hyperalgesia. The choice of the analgesics was based on pain mitigating mechanisms utilized by common analgesics including, activation of peripheral opioid receptors, decreased intracellular calcium concentration, and activation of the TRPV receptors. The broad category of anti-inflammatory agents was left out of this study since the variability in tumor inflammation was considered too diverse across cancer types and would likely warrant a separate study.

2. Methods

2.1. Animal care

The study was conducted using protocols approved by the Institutional Animal Ethical Committee, Amrita Institute of Medical Sciences, Kochi, India in accordance with guidelines set forth by the Committee for the Purpose of Control and Supervision of Experiments on Animals, Government of India. Adult female Sprague–Dawley (SD) rats weighing 200–250 g were housed in pairs, allowed standard rat diet and water ad libitum, and maintained in 10 h/14 h light/dark cycle.

2.2. Rat model of cancer-induced bone pain

Experimental model of bone tumor was induced in female SD rats by injecting allogenic breast cancer cell line, MRMT1 (Riken, Japan) into the proximal end of tibia, as previously described (Mathew et al., 2020). Briefly, almost confluent MRMT1 cells were trypsinized, washed and resuspended in HBSS at a concentration of 3×10^7 cells/mL. Cells were maintained at 4 °C and administered to animals the same day. Prior to tumor-cell inoculation, rats were anesthetized by intraperitoneal injection of ketamine (100 mg/kg) – xylazine (5 mg/kg), followed by inhalational 1–2% isoflurane that was maintained throughout the procedure. A small 5–8 mm skin incision was applied on the anteromedial surface of the left knee joint to allow penetration of a 24-gauge needle into the proximal end of the tibia. Care was taken to gently advance the needle through the articulating cartilage and enter only about 2–3 mm of the underlying bone. MRMT1 cell suspension (10 μL) was gradually injected using a graduated Hamilton syringe, followed by wound closure and post-surgical recovery. Animals in the sham group received heat inactivated MRMT1 cells. All animals were monitored for palpable tumor mass and euthanized 2–3 weeks post tumor induction.

2.3. Radiography of rat limb

Hind-limbs of anesthetized animals were radiographically imaged (GE OEC 9600 C-Arm, USA) on 14-day PTI, and the radiograms were analyzed by a blinded observer.

2.4. Micro-CT imaging

Excised ipsilateral and contralateral rat hindlimbs from euthanized animals were collected, fixed with 4% (w/v) paraformaldehyde, washed with 0.1 M PBS, gently wiped and placed in a cylindrical sample holder. Microcomputed tomography scanner (MILabs, Netherlands) was used to scan tibia with 8.8 voxel size, and 3D reconstructions were carried out with a dedicated visualization software (MILabs, Netherlands) and ImageJ software. Acquired images were analyzed by a blinded observer.

2.5. Peri-tumoral administration of pharmacological agents

Pharmacological agents were administered to tumor-burdened rats under a very short inhalational exposure to 1–2% isoflurane. Drugs were administered via a 1 mL U-40 insulin syringe, that was inserted along the periphery of the tumor mass at different sites. The injection site was digitally palpated during needle insertion and care was taken to inject the drugs primarily into the bone around the tumor, without any infiltration into the tumor mass. The total volume of the injectate was maintained at 200 μL for all drugs. DPDPE (0.04 and 0.4 mg/kg; Abcam, USA), ziconotide (0.0015 and 0.015 mg/kg; Alomone labs, Israel), diltiazem (2 and 20 mg/kg; Abcam, USA), mibefradil (0.25 and 2.5 mg/kg; Tocris, UK) drug solutions were prepared in sterile saline according to the manufacturer's protocol. JNJ-17203212 injectate (0.5 and 5 mg/kg; Tocris, UK) was prepared in 10% DMSO, 40% PEG400, 5%Tween-80 and 45% saline. Animals received the pharmacological agents individually or in combination on day 14 PTI, followed by behavioral studies to test pain sensitivity. To control for systemic dissemination of injected drugs, tumor-burdened rats received intra-articular injections in the contralateral limb, or drugs were administered via the peritoneal route. Effectiveness of administered analgesics was quantified as a percentage of maximum possible effect (%MPE) calculated as below (Afify and Andijani, 2017).

$$\%Maximum\ \ possible\ \ effect\ \ (\%MPE) = \frac{Measured\ \ baseline - Tumor\ \ baseline}{Maximum\ \ baseline - Tumor\ \ baseline} * 100$$

In addition, the duration of analgesia was calculated as the time up to which the animals maintained an MPE of 50% or more. All animals were tested for a minimum of 2hrs after drug injection and testing was continued until the pre-drug baseline was achieved. Animals received drug injections after a gap of 24–48hrs after experimental sessions.

2.6. Pain studies

Behavioral responsiveness to pressure, tactile, and thermal, stimuli were measured in rats, once every three days, till the end of the study.

Pressure stimulus: Limb withdrawal thresholds (LWT) were measured by applying a gradually increasing pressure stimulus (Pressure application meter, Ugo Basile, Italy) around the knee joint. A pressure transducer strapped to the investigators thumb, was used to apply force at the rate of 300 g/s. The application of stimulus was stopped when the animal demonstrated limb withdrawal, or remained unresponsive for 5 s, whichever occurred earlier, and the peak gram force eliciting the response recorded as the LWT. Recordings were repeated thrice on each limb, with a 5 min interval between each recording and the mean value calculated.

Tactile stimulus: Tactile mechanical stimulus was applied to the mid-plantar surface of the hind paw of acclimatized rats placed on a wire-mesh bottom platform, using a hand-held force transducer fitted with an 8 mm semi-flexible polypropylene tip (electronic von Frey anesthesiometer, IITC Inc., Life Science Instruments, Woodland Hills, CA, USA). Reflexive withdrawal of the paw in response to the application of an increasing perpendicular force along the polypropylene tip for 4 s, was recorded as a positive response. The application of stimulus was stopped when the animal demonstrated paw withdrawal, or remained unresponsive after 4 s, whichever occurred earlier. The peak force eliciting the response was recorded as the paw withdrawal threshold (PWT). Recordings were repeated four times per limb and the mean value calculated.

Thermal stimulus: Thermal responsiveness was quantified using a microprocessor- controlled hot plate (IITC Life Sciences, USA). The hind paw of acclimatized animals was gently placed on the surface of the hot plate heated to 56 °C with a cut-off period of 10 s. The time taken by the animal to reflexively remove its limb from the heated surface was recorded. Each limb was alternated three times, and the mean value considered as the paw withdrawal latency (PWL).

Extensor postural thrust: Extensor postural thrust was assessed to determine lower motor strength in lower limbs. Rats were held over a digital weighing balance, where the animal was allowed to bear weight on one hind paw at a time. The maximum weight borne by the limb was recorded. Each recording was repeated three times, and the mean value considered as the extensor postural thrust.

2.7. Ratiometric calcium imaging in DRG neurons

Rats were euthanized by CO_2 asphyxiation, and a lumbar laminectomy was performed. Lumbar dorsal root ganglions (L1 to L5) were carefully identified, extracted, and quickly immersed in ice-cold Ca^{2+} and Mg^{2+} free Hank's Balanced Salt Solution (Lonza, USA). Further, DRG's were dissociated using a modified procedure as previously reported (Shankarappa et al., 2011). Briefly, each DRG was cut into 2–3 pieces and incubated in collagenase (2 mg/ mL; type I, Invitrogen) and dispase (5 mg/mL; type II, Invitrogen) cocktail at 37 °C for 25 min, under shaking conditions. Enzymatically digested DRG tissues were then washed with HBSS, triturated 10–15 times using a glass pipette with a tapered end, and subsequently seeded on poly-D-lysine (100 μg/mL) coated glass coverslips (ø12mm) in medium containing DMEM with 10%(v/v) Ham's F-12 supplement, 10%(v/v) FBS, and 1% (v/v) PS (Katiyar et al., 2021). DRG cells were incubated at 37°C in 5% CO_2 for at least 2hrs before ratiometric imaging. All imaging procedures were completed within 6–8 hrs from tissue harvest. To assess intracellular calcium concentration, DRG neurons were loaded with 1 μM FURA-2AM (Thermo Fisher Scientific, USA) for 30 min at 37 °C and washed with Ca^{2+} and Mg^{2+} free Tyrode's solution (Alfa Aesar, USA) and placed in dark for additional 30 min for dye de-esterification at RT. Coverslips were placed on an imaging chamber (Warner instruments, USA) and super-fused with Ca^{2+} and Mg^{2+} free Tyrode's solution maintained at RT using a gravity-assisted perfusion controller, and cells were imaged at 200 times magnification under an inverted fluorescent microscope connected to a CCD camera (Leica DFC3000G, Germany). Visually healthy, small, and medium diameter DRG neurons were marked as regions of interest for measuring 'R′ values within the ratiometric fluorescence imaging software (Metafluor, Molecular Devices, USA), after appropriate background subtraction. Images were captured at 510 nm with excitation wavelength of 340/380 nm. All imaging parameters including exposure time, gain and time-intervals were maintained constant throughout the experiment. Intracellular Ca^{2+} response was elicited by perfusing 25 mM KCl, with or without the specific pharmacological agents (DPDPE, ziconotide, diltiazem, mibefradil and JNJ-17203212) in the bath solution. Intracellular Ca^{2+} levels were calculated using the equation:

$$(Ca^{2+})i = K_d \times Q \times \frac{(R - R_{\min})}{(R_{\max} - R)}$$

(where, R_{min} 0.09, R_{max} 8.43, Q 32.62, and K_d 45, obtained using Fura-2 calcium imaging calibration kits (Invitrogen, USA) were used for all ratiometric experiments).

2.8. Immunohistochemistry

Dorsal root ganglia (DRG) were harvested from day 14 naïve, sham and tumor-bearing rats were utilized to determine the expression levels of peripheral delta opioid receptor (DOPr), calcium channel ions (N-type; CACNA1B), (L-type; CACNA1C) and TRPV1 ion channels (TRPV1) respectively. Ipsilateral and contralateral tibial bone from 14-d CIBP animals were used to determine CGRP positive nerve fiber expression. Animals were trans-cardially perfused with 0.9% (w/v) heparinized saline and fixed with 4%(w/v) paraformaldehyde in 0.1 M PBS. Bone and intact dorsal root ganglia were identified, excised carefully and post-fixed with 4%(w/v) paraformaldehyde overnight. Fixed DRG tissues were dehydrated using increasing concentration steps of ethanol, embedded in paraffin blocks and 5 μm thin sections cut using a microtome (Thermo Fisher Scientific, USA). Thin slices of tibial bone were prepared using marathon clinical micro-motor unit (Saeyang Microtech, South Korea) attached to a diamond disc blade and post-fixed with 4% (w/v) paraformaldehyde overnight. Bone tissue were de-calcified by immersing in 6%TCA solution for 3–4 days at 4 °C and then washed with 0.1 M PBS. Ethanol dehydrated bone sections were embedded in paraffin blocks and 7–10 μm thin sections were cut using a microtome. Additionally, bone section (3 sections per slide) were subjected to heat induced antigen retrieval for 10 min at 100 °C, stained with rabbit polyclonal anti-CGRP antibody (1:200; Abcam, USA and counterstained with DyLight 549 conjugated secondary antibody (10 μg/mL) (Vector Labs, USA). Nerve fiber quantification was performed on 3 tissue sections per group, harvested from 3 rats. Three to ten non-overlapping images per section were selected, and nerve fiber identification, length measurement and beading was performed using ImageJ software. All DRG sections were rehydrated and stained with rabbit polyclonal anti-DOPr antibody (1:100; Abcam, USA), rabbit polyclonal anti-CACNA1B antibody (1:200; Abcam, USA), rabbit polyclonal anti-CACNA1C antibody (1:200; Alomone labs, Israel) and rabbit polyclonal anti-TRPV1antibody (1:200; Abcam, USA) and counterstained with DyLight 549 conjugated secondary antibody (10 μg/mL) (Vector Labs, USA). For quantification of ipsilateral and contralateral lumbar DRG protein expression, analysis was performed on 3 tissue sections per group, harvested from 4 to 8 rats. Three to ten non-overlapping images per section were selected, and fluorescence intensity measured in approximately 50–400 neurons per group. All tissue sections were examined using Leica 3000B inverted fluorescent microscope connected to a CCD camera (Leica DFC3000G, Germany). Each DRG neuron was specified with a region of interest (ROI) and fluorescence intensity was quantified using ImageJ software and displayed as normalized corrected total cell fluorescence (CTCF) (do Couto et al., 2020).

$$CTCF = (Integrated\ \ density\ \ ) - (Area\ \ of\ \ selected\ \ cell\ \ x\ \ Mean\ \ fluorescence\ \ of\ \ backround\ \ readings)$$

A neuron was considered positive for the protein expressed, if the normalized CTCF value was 50% higher than their respective IgG control. Further, percentage DOPr, CACNA1B, CACNA1C, TRPV1 positive cells were calculated by counting the total number of cells and the number of positive cells per field.

2.9. Total RNA isolation and cDNA synthesis

Total RNA was isolated from DRG tissue obtained from naïve and CIBP animals. Additionally, total RNA was extracted from Day 5 DRG cultures treated with 50% tumor conditioned media. RNA extraction was performed as per manufacturer's protocol using the Nucleospin® RNA Plus kit (740984, Takara Bio, Japan). RNA purity was determined based on the ratio of absorbance between 260 and 280 nm using the NanoDrop® spectrophotometer, and only samples with ratio values exceeding 2.0 were further processed. The cDNA synthesis was performed using the PrimeScript RT Reagent Kit (RR037A, Takara Bio, Japan), following the manufacturer's protocol, on a CFX96 Real-Time system thermal cycler (Bio-Rad, USA), and stored at − 20 °C until further use.

2.10. Quantitative real-time PCR

Quantitative RT-PCR (qRT-PCR) was performed using the TBGreen Premix Ex *Taq*II (RR820A, Takara Bio, Japan) as per the manufacturer's protocol. Primers were preformulated for DOPr, TRPV1, CACNA1B, CACNA1C, CACNA1H and housekeeping gene (β-actin) (Table 1). The thermal cycling conditions for amplification consisted of an initial denaturation step at 95 °C for 3 min, followed by 40 cycles of denaturation at 95 °C for 30 s, and annealing and extension at 65 °C for 20 s for TRPV1, CACNA1C, and CACNA1B, and at 68 °C for DOPr and CACNA1H. All RT-qPCR experiments were performed on CFX96 Real-Time system thermal cycler (Bio-Rad, USA). Relative mRNA expression level was calculated by 2-ΔΔCq (Livak) method where CT of target gene was normalized to that of reference gene (β-actin) for both test and calibrator samples.

2.11. Statistics

Difference in mean values between experimental and control groups have been tested using GraphPad Prism version 9.4 for Mac (GraphPad Software, La Jolla California USA). Individual statistical tests are indicated in each figure legend.

Table 1
Pre-formulated primer sequences used for qRT-PCR.

Sl.No	Targets	Primer sequence
1	DOPr	sense 5′-TGAAGACGGCCACCAACATCTACA-3′ anti-sense 5′-TTTCCATCAGGTACTTGGCGCTCT-3′
2	TRPV1	sense 5′-AGCCAACGCAAGGAGTATGTG-3′ anti-sense 5′-CAGTAACAGGATGATGAAGACAGC-3′
3	CACNA1B	sense 5′-AGGCCAGACATGAAGACACACA-3′ anti-sense 5′-TTGCCTTCCTTGCTTGAGTCCT-3′
4	CACNA1C	sense 5′-CAGCTGTTTGGTGGAAAGTTCA-3′ anti-sense 5′-TGTTGATCTTGGTAGTGGGTGG-3′
5	CACNA1H	sense 5′-ATCAATCCCACCATCATCCGCA-3′ anti-sense 5′-ACCTTGGCT TTCCTGTGCTGTA-3′
6	β-Actin	sense 5′-CCGTGAAAAGATGACCCAGA-3′ anti-sense 5′-GTCTCCGGAGTCCATCACAA-3′

3. Results

3.1. Osteolysis and pain behavior in the CIBP rat model

Allogenic breast cancer cells were injected into the proximal part of the left tibial bone, just underneath the articulating cartilage in female SD rats. After 4–6 days post tumor induction (PTI), a distinct solitary palpable nodule at the injection site was observed, that gradually increased in size to a large mass over the next 6–10 days (Suppl. Fig. 1a). Gross examination revealed a smooth tumor mass with soft consistency that was fixed to the underlying bone. The skin over the mass appeared normal with no apparent redness or ulceration and was not fixed to the tissue below. Excised tibia from 14 d PTI rats demonstrated loss of normal bone structure with significant tissue erosion (Fig. 1a). Radiographs of the knee joint obtained from day 14 PTI rats showed translucent lytic lesions within proximal tibia, along with outline of the tumor soft tissue shadows (Fig. 1b). Micro-CT images of the tumor-bearing bone further confirmed the presence of multiple, lytic lesions that had eroded the articulating surface of the proximal tibia (Fig. 1c and d). Smaller lytic lesions were also observed in inner medial regions near the articulating surface of the femur (Fig. 1d), most likely due to the extravasation of the tumor cells into the knee joint. Histological analysis of bone sections harvested from the lesion site showed infiltration of tumor cells within the cortical and trabecular bone (Fig. 1e and f), along with loss of normal bone morphology. In pain behavioral studies, compared to rats receiving heat killed MRMT1 cells (sham), those receiving viable MRMT1 cells demonstrated enhanced responsiveness to pressure stimulus applied at the tumor site (knee) ($P < 0.05$, n = 8–16, Fig. 1 g), suggestive of local pressure hyperalgesia. Primary pressure hyperalgesia in the ipsilateral limb was observed starting on day 6 and was maintained throughout the duration of the study. Additionally, animals showed increased tactile responsiveness upon mechanical probing of the hind paw in the tumor-affected limb compared to sham animals ($P < 0.05$, n = 8–16, Fig. 1 h), suggesting distal hyperalgesia. The onset of distal hyperalgesia was also observed around day 6 and remained throughout the duration of the study. In contrast, animals demonstrated similar thermal responsiveness in tumor-burdened limb compared to the tumor-free limb ($P < 0.05$, n = 8–16, Fig. S1c). Interestingly, despite the aggressive nature of the induced tumor, rats appeared active, with no loss in body weight (Fig. S1b). In addition, the extensor postural thrust (EPT), a commonly used measure of motor strength showed transient reduction shortly following tumor induction but recovered in the following week ($P > 0.05$, n = 8–16, Fig. S1d). There was also no visible change in gait throughout the period of study, and all animals could easily bear weight on the tumor affected limb, suggesting that tumor induction most likely did not affect overall limb motor function. Gait analysis was not performed in this study.

3.2. Expression of mRNA and receptor proteins associated with pain-signaling in lumbar DRG cell bodies of CIBP rats

Specific pain-signaling associated receptor expression within lumbar DRG sensory neurons innervating the tumor site was determined in CIBP rats by immunohistochemical analysis. The lumbar L1-L3 DRG's were chosen since axons innervating the epiphyseal region of the tibia (Matsuo et al., 2019) arise from neuronal cell bodies located in these spinal segments, while L4-L5 segments innervate the distal hind paw.

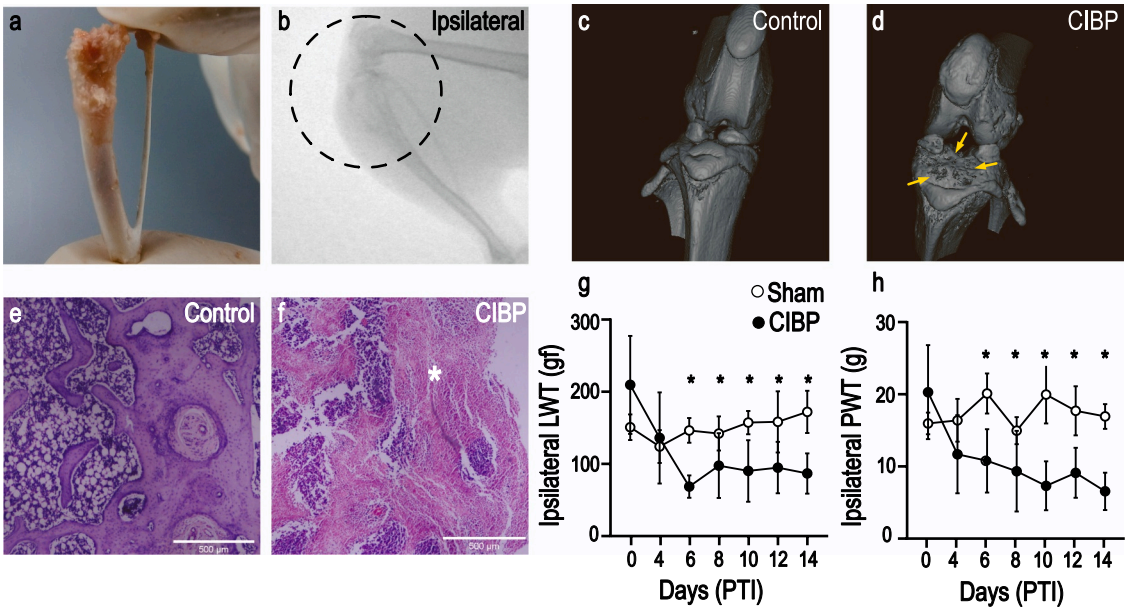

Fig. 1. Tumor induced alteration in local bone architecture and pain behaviour in rats with CIBP. The proximal end of tibia injected with MRMT1 cells demonstrated bony erosion and matrix destruction on gross examination after 14-d post tumor induction (a). Radiographs showed lytic lesions within the bone along with soft tissue mass (b), while micro-CT showed osteolytic lesions (arrows) on the articulating surface in the tumor affected knee (d). Haematoxylin and eosin staining of tumor affected bone sections revealed infiltration of tumor cells (star symbol) into cortical and trabecular bone regions (scale bar = 500 μm) (e, f). In pain studies, local pressure application at the primary tumor site (knee) evoked sharp limb withdrawal response (g), while tactile-stimulus application to the ipsilateral hind paw resulted in reflexive paw withdrawal (h). Data shown are mean ± SD of calculated withdrawal threshold values, obtained from ipsilateral limbs of CIBP (n = 16) and sham rats (n = 8). * indicates P value of < 0.05, multiple t-test using Holm-Sidak method.

The harvested DRGs were analyzed for expression of DOPr, N-type Ca^{2+} channel (CACNA1B), L-type Ca^{2+} channel (CACNA1C) and TRPV1 protein in neuronal cell bodies. IgG rabbit antibody was used as isotypic control, and DRG tissue sections from naïve and sham animals were used as comparative controls. Neurons exhibiting fluorescent intensity values that were more than 50% of controls, were determined as positive for the probed protein, and the overall fluorescent intensity was quantified and expressed as corrected total cell fluorescence (CTCF) units. DRG tissue sections immuno-stained for peripheral DOPr, demonstrated fluorescent signals from neuronal cytoplasm and multiple axonal segments (Fig. 2b-d). About 30% of neurons in the L1–3 DRG, and about 50% neurons in the L4–5 DRG were found to be positive for DOPr in CIBP animals, while naïve and sham controls had less than 10% positive cells, although the difference between means did not reach statistical significance (Fig. 2e). Importantly, compared to controls, the overall CTCF values in the CIBP groups showed no significant difference ($P > 0.05$) (Fig. 2 f). DRG sections stained for the N-type Ca^{2+} channel protein, showed similar immunostaining profile in CIBP rats compared to controls (Fig. 2i-k), while sections stained for the L-type Ca^{2+} channels showed slightly higher positivity in the L4–5 DRGs for all groups (Fig. 2p-r). There was no significant difference in fluorescent intensity between control and CIBP groups that were stained for TRPV1 protein antibody, although the number of positive cells were slightly higher in the CIBP group (Fig. 2z). Additionally, we observed that expression of DOPr, CACNA1B, CACNA1C and TRPV1 genes from DRGs that were either harvested from CIBP rats, or treated with tumor conditioned medium, was similar to controls (Fig. 2 g, n, u, ab; Fig. S5). Overall, these results suggest that bone tumor in the proximal tibia did not significantly affect the expression of DOPr, N-, L- type calcium channel and TRPV1 receptor proteins and mRNA in DRG neurons.

3.3. Nerve fiber distribution in tumor-burdened bone tissue

We next asked if nerve innervation was disrupted by tumor induction within tibia and examined neurite distribution after staining for calcitonin gene related peptide (CGRP) (Fig. 3a-d). Despite the presence of tumor cells, distinct nerve fibers were observed within the bone tissue. Overall, nerve fibers were detected in the cortical bone and close to the bone marrow, while a clear delimiting periosteal layer was not visible. The absence of periosteum could likely be due to periosteal damage and erosion caused by infiltrating cancer cells. The immunostained nerve fibers were seen as individual tortuous structures with a beaded appearance (Fig. 3d). The innervation was moderately dense with no specific patterns and did not show any histological signs of neurite injury. The tumor-burdened tissue exhibited a reduction in the number of nerve fibers relative to contralateral tissue sections (Fig. 3e). However, nerve fiber length, beading pattern and beading density on the nerve fibers, indicative of injury, were similar (Fig. 3 f, g) in both groups. These results confirm the presence of intact sensory nerve fibers, albeit reduced, within tumor-burdened bone tissue.

3.4. Effect of antinociceptive agents on intracellular Ca^{2+} response in DRG neurons from CIBP animals

To determine the sensitivity of pain neurons to antinociceptive agents, we measured alterations in calcium homeostasis in sensory neurons innervating the tumor site. Small and medium diameter neurons isolated from L1–L5 DRGs from tumor-bearing, and naïve rats were subjected to ratiometric Ca^{2+} imaging. Analysis of calcium transients demonstrated resting intracellular $(Ca^{2+})_i$ concentration that was about 40% higher in DRG neurons from CIBP animals (89 ± 49 nM; n = 598), compared to controls (63 ± 17 nM; n = 28) (Fig. 4a). Following KCl-induced depolarization, neurons from CIBP animals demonstrated peak $(Ca^{2+})_i$ response (227 ± 185 nM; n = 134) that was about 32% higher than controls (171 ± 112 nM; n = 24) (Fig. 4b). To further determine $(Ca^{2+})_i$ response to selected antinociceptive agents, DRG neurons harvested from CIBP rats were independently perfused with DOPr agonist [D-Pen^{2,5}] -Enkephalin (DPDPE), N-type Ca^{2+} channel antagonist (ziconotide), L-type Ca^{2+} channel antagonist (diltiazem), T-type Ca^{2+} channel antagonist (mibefradil) and TRPV1 channel

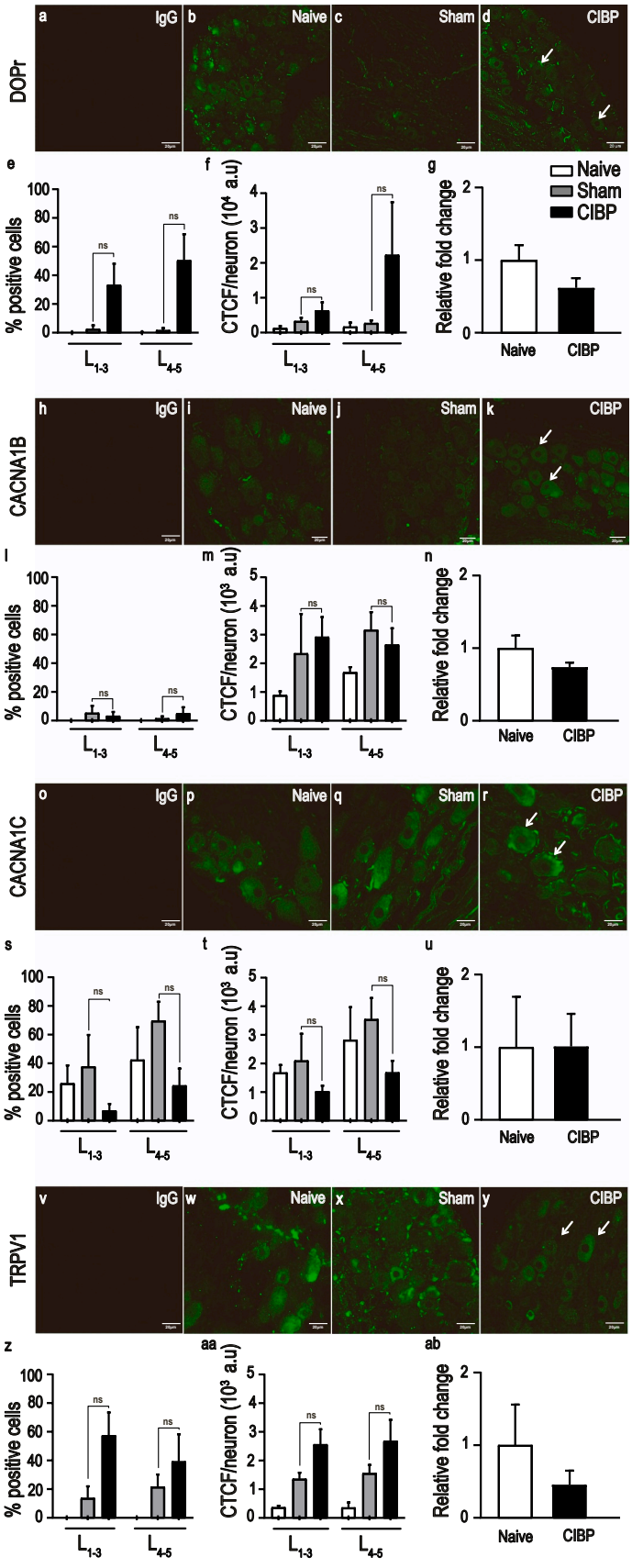

Fig. 2. Protein and mRNA expression of DOPr, CACNA1B, CACNA1C and TRPV1 in DRG neurons. Typical immunohistochemical images depicting DOPr (b-d), CACNA1B (i-k), CACNA1C (p-r) and TRPV1-positive cells (w-y) (arrows), from ipsilateral lumbar (L1–3 & L4–5) DRG sections harvested from CIBP (14-d PTI, n = 8), sham (n = 4) and naïve rats (n = 4). Protein expression was quantified and represented as percentage positive cells (e, l, s, z) and corrected total cell fluorescence (f, m, t, aa) for each protein and data expressed as mean ± SEM. The IgG control antibody was raised in rabbit (a, h, o, v). mRNA expression was quantified relative to naïve control group and shown as mean ± SD (g, n, u, ab). Statistical analysis was performed using one-way ANOVA with Sidak's multiple comparison (for protein expression), and unpaired Student's t-test with Welch's correction (for mRNA expression).

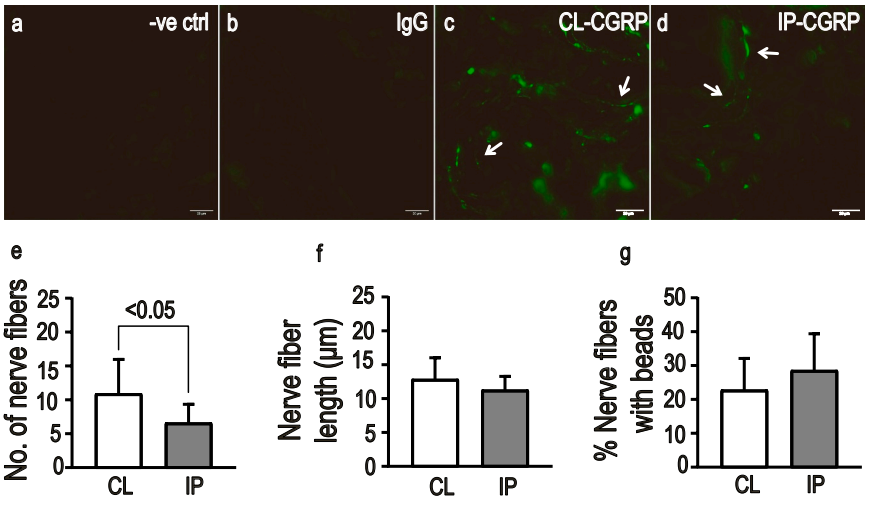

Fig. 3. Identification of nerve fibers within bone tissue. Representative immunohistochemical images showing CGRP+ve nerve fibers (arrows) from decalcified tibial bone sections harvested from ipsilateral (d) and contralateral site (c) of 14-d PTI rats. Negative control with no primary antibody (a) and isotype control (b) were utilized to validate antibody specificity. Bar graphs indicating average number of CGRP+ve nerve fibers (e), nerve fiber length (f), and percentage of nerve fibers with beaded appearance (g), obtained from contralateral (CL) and ipsilateral (IP) tibial bone sections from CIBP rats (n = 3). Data shown as mean ± SD; from measurements performed in at least 3 sections per rat. Statistical analysis was performed using an unpaired t-test with Welch's correction, and P value indicated as above.

antagonist (JNJ-17203212) for 10 min. Basal and peak $(Ca^{2+})_i$ response was recorded and the efficacy of perfused drugs in reducing peak $(Ca^{2+})_i$ response was calculated. DPDPE exhibited a dose-dependent reduction in peak $(Ca^{2+})_i$ levels with 100 nM (110 ± 91 nM; n = 20) and 1000 nM (102 ± 61 nM; n = 20) showing 50% efficacy in reducing peak $(Ca^{2+})_i$ (Fig. 4c) compared to non-perfused controls (227 ± 185 nM; n = 134) ($P < 0.05$). Similarly, perfusion of 1000 nM of ziconotide, diltiazem and JNJ-17203212 induced approximately 40% reduction in peak $(Ca^{2+})_i$ response, while mibefradil had no effect (Fig. 4d, e, f, g). Furthermore, combination of DPDPE with other agents produced peak $(Ca^{2+})_i$ responses that were no different from individually tested drugs (Fig. 4h), suggesting that the drug combinations tested in this study did not provide additional benefits.

3.5. Drug-induced pain attenuation at primary and distal tumor sites in CIBP rats

To assess the antinociceptive effects of analgesics administered in the peri-tumoral area, evoked pain behavior response to graded mechanical pressure and tactile stimulus was tested at the tumor site and the hind paw respectively, in day 14 PTI rats. Effectiveness of administered analgesics was quantified as a percentage of maximum possible effect (% MPE), along with the total duration of analgesia. Animals exhibiting MPE of more than 50% were considered as responders, but data was analyzed inclusive of both responders and non-responders. Peri-tumoral administration of DPDPE at lower (0.04 mg/kg) and higher (0.4 mg/kg) dose reduced primary pressure hyperalgesia in approximately 50% and 75% of the animals respectively (Fig. 5 & Table S1). Lower dose of DPDPE attenuated primary pressure hyperalgesia with an MPE of 71 ± 11% for about 37 ± 48 min while, a higher dose resulted in an MPE of 84 ± 21% for 81 ± 54 min (Table S1). Similarly, the centrally mediated distal hyperalgesia was also reduced after peritumoral DPDPE administration in approximately 50% of the animals tested (Fig. 6 & Table S2). Intrestingly, intra-articular injection of DPDPE in the contralateral limb showed pain mitigating effect at the centrally mediated distal site, but not as much at the local site (Fig S3). Expectedly, systemically administered DPDPE controls produced primary and distal analgesia that was quite robust and comparable to that obtained by DPDPE administered via the peritumoral route (Fig. S4). Overall, local peritumoral administration of δ-opioid agonist showed robust attenuation of primary pressure hyperalgesia, but the observed mitigation of distal hyperalgesia could most likely be due to systemic leakage from the injected site.

Similarly, pain responses after peritumoral application of ziconotide (0.0015 mg/kg; 0.015 mg/kg), diltiazem (2 mg/kg; 20 mg/kg), mibefradil (0.25 mg/kg), and JNJ-17203212 (5 mg/kg) were tested in rats with CIBP. Attenuation of primary pressure hyperalgesia and distal hyperalgesia were mostly comparable with controls ($P > 0.05$) suggesting that peritumoral administration of Ca^{2+} channel and TRPV1 antagonists does not play a significant role in attenuating CIBP (Figs. 5 and 6). Interestingly, higher dose of mibefradil (2.5 mg/kg) showed significant reduction in primary pressure hyperalgesia ($P < 0.05$).

4. Discussion

Peripheral nerve fibers in the vicinity of cancer lesions are one of the least explored components of the tumor microenvironment. Lately, studies have focused on the functional role of cancer nerve terminals and found that axonal terminals in the tumor microenvironment alter cancer growth, and possibly promote metastasis (Jerard et al., 2023). In fact, there appears to be strong two-way cross talk between tumor cells and the peripheral nerve terminals, with each affecting the other in multiple ways (Silverman et al., 2021). In this scenario, it is important to understand how such nerve terminals exposed to a highly heterogenous and cytokine-rich tumor microenvironment responds to local application of select analgesics. Especially with the recent development in prolonged and sustained drug delivery system technologies, it is quite plausible that guided or unguided local infiltration analgesia could be further expanded for managing cancer pain in palliative settings.

In this study, we attempt to address this issue by exploring the responsiveness of nerve terminals to select analgesic drugs in a model of cancer induced bone pain. The analgesics were chosen based on pain mitigating mechanisms utilized by common analgesics including, activation of peripheral opioid receptors, decreased intracellular calcium concentration, and activation of the TRPV receptors. To test the effect of these analgesics on CIBP, we utilized an allogenic rat model that showed robust tumor growth along with primary and distal hyperalgesia in response to intraosseous administration of breast cancer cells. Compared to other bone cancer models that administer cancer cells into the medullary compartment of long bones through a pre-drilled opening (Urch et al., 2003), in this study we implemented a relatively simpler, yet reproducible procedure where cancer cells are injected into the cortico-trabecular area just underneath the articulating cartilage of the proximal tibia. Because tumor growth is quite apparent and easily accessible by palpation, identification of tumor margin for peri-tumoral injection is quite simple and accurate. Furthermore, since the tumor growth was consistently in the superior part of the tibia encroaching on the articulating surface, the specific DRGs innervating the anatomical area could be reliably targeted and isolated. However, in addition to sensory afferents, several sympathetic fibers arising from the thoracolumbar sympathetic ganglia innervate the condylar region of the

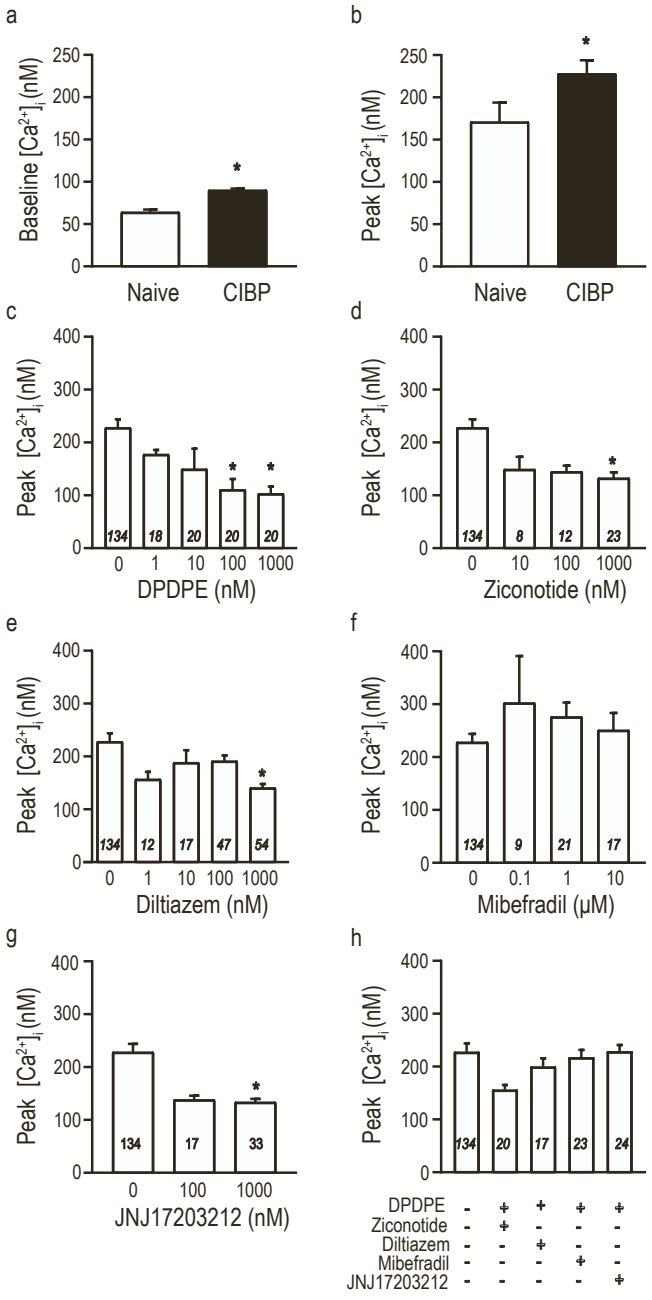

Fig. 4. Intracellular calcium response in sensory neurons innervating bone tumor. Bar graphs showing intracellular Ca^{2+} concentration at rest (a), and peak Ca^{2+} after KCl-induced depolarization (b) in small and medium sized DRG neurons harvested from naïve (n = 28 neurons), and CIBP rats (n = 598 neurons) . Peak Ca^{2+} levels from neurons exposed to varying concentrations of DPDPE (c), Ziconotide (d), Diltiazem (e), Mibefradil (f), JNJ-17203212 (g), along with drug combinations (h) were quantified. Individual drug concentration used in (h) was 100 nM for all drugs. Data shown as mean ± SEM, where the number of neurons tested per group is indicated within each bar graph. Statistical analysis was performed using Student's-test with Welch's correction (a,b), and one-way ANOVA with Sidak's multiple comparison test (c-h), * indicates P value of < 0.05.

knee (Matsuo et al., 2019) and partially contribute to hyperalgesia associated with nerve injury, but these ganglia were not examined in this study.

Behaviourally, CIBP manifested as localized pain at the tumor site, and distal pain at the hind paw. The local pain response elicited by a graded pressure stimulus at the tumor site could be attributed to the activation of peripheral nerve fibers in or around the tumor. Interestingly, our immunohistochemical analysis of the tumor site revealed a marked reduction in the number of nerve fibers within the tumor area, although there was no difference in the overall length of existing nerve fibers or fiber beading. It is interesting to consider that experimental tumor models are generally quite aggressive and may not allow sufficient time for adaptive changes to occur in innervating nerve fibers. The reduced number of nerve fibers per tissue section could also be due to displacement of innervating fibers by the fast-growing tumor cells. Our observation related to reduced nerve density in the tumor site is consistent with previous reports in pancreatic (Iwasaki et al., 2019), and endometrial cancer (Giray et al., 2018). In addition, some studies have reported hypertrophy of nerve terminals at the tumor site (Zhao et al., 2014), but this feature was not examined in this study. Additionally, the distal hyperalgesia observed in this study is also consistent with other medullary bone cancer pain models and is commonly attributed to central sensitization in dorsal horn neurons (Latremoliere and Woolf, 2009). However, it is important to note that in some reports, the term 'secondary hyperalgesia' has been used in overlapping context with distal hyperalgesia, to describe pain sensitivity in remote areas, as well as in the neighbouring vicinity of the primary pain source (Sandkühler, 2009; Jochmann et al., 2015). In our study, the elicited paw withdrawal response is remote from the tumor site, and as reported earlier, it is associated with increased expression of ATF3 (Mathew, Madhusudanan and Shankarappa, 2020) in central neurons, suggestive of central sensitization. Due to these reasons, we have described the observed remote paw-withdrawal response as CIBP-induced distal sensitivity or hyperalgesia, to maintain distinction.

Cell bodies of neurons innervating the tumor area clearly demonstrated expression of DOPr, N-, L-type Ca^{2+} channels, and TRPV1 proteins, and this observation was consistent with previous reports that validate their distribution in peripheral sensory neurons and spinal cord (Fuchs et al., 2007; Otis, Sarret and Gendron, 2011; Li et al., 2015). However, we found no changes in the expression of the tested receptor proteins in the DRG's of CIBP animals using immuno-histochemical methods, although few previous studies have observed increased DOPr mRNA and protein levels in chronic inflammatory pain conditions (Cahill et al., 2003). Since cancer pain has features of both inflammatory and neuropathic pain (Urch, 2004), and the tumor environment is commonly infiltrated by inflammatory cells, we had hypothesized that receptors associated with pain signalling would be increased. However, we did not observe any change in receptor protein and mRNA expression, suggesting that tumor induction in the bone did not affect the expression of our targeted proteins. Even though we detected expression of DOPr in the cell bodies of sensory neurons, the anti-DOPr antibody utilized in this study showed poor binding within bone tissue, possibly due to harsh antigen retrieval procedures and decalcification methods adopted in immunohistochemical methods for bone. Detection of DOPr in bone tissue has proved to be quite difficult and even sensitive methods such as radio-ligand binding assays require pooled tissue samples for identification (Bergströmmm et al., 2006).

Since intracellular Ca^{2+} response to evoked depolarization is a well-established cellular indicator of pain modulatory mechanisms in sensory neurons, we used ratiometric imaging technique to further determine the efficacy of each of the drug targets in DRG neurons from CIBP animals. Two weeks post tumor induction, we observed both resting and evoked peak Ca^{2+} concentration to be significantly higher in lumbar DRG neurons, compared to non-tumorigenic animals. Interestingly, conditioned media obtained from rhabdomyosarcoma and osteosarcoma cells has been shown to increase intracellular calcium concentration in healthy neurons via activation of TRPV1 channels (Lautner et al., 2011). In animal experiments, DRG neurons harvested from mice with fibro-sarcomatous tumours demonstrated increased intracellular Ca^{2+} levels, along with enhanced activity of voltage-gated Ca^{2+} channels (Khasabova et al., 2007). Increased intracellular Ca^{2+} levels in primary afferent neurons from tumor burdened animals has been

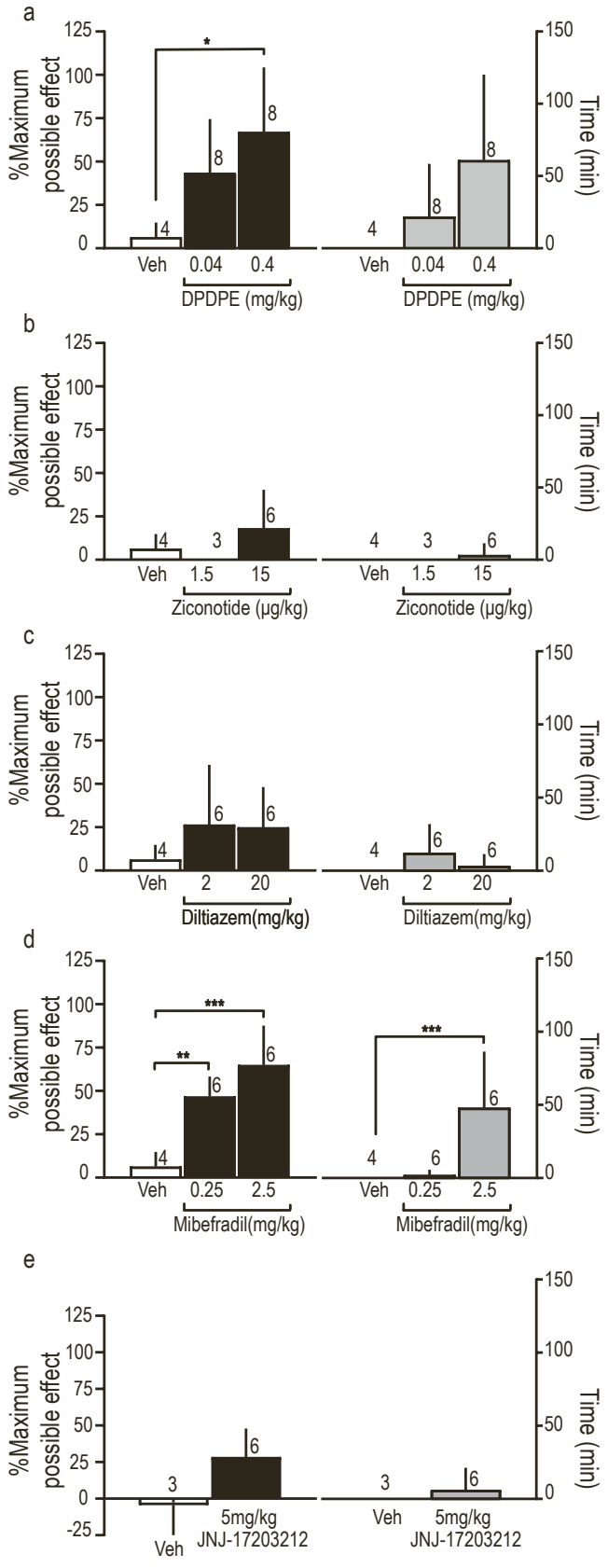

(caption on next column)

Fig. 5. Pain attenuation at tumor site. The antinociceptive effect of analgesics administered via the peritumoral route was expressed as percent of maximum possible effect (MPE) (left Y axis, black bars). Duration of analgesia was calculated and quantified (right Y axis, grey bars). All behavioral responses were measured from the tumor site at the knee, after application of a graded mechanical pressure stimulus. Data shown as mean ± SD where number of rats tested per group is indicated on top of the bar graph. Statistical analysis was performed using one-way ANOVA, with Dunnett's multiple comparison test compared to vehicle group, * indicates P value of < 0.05.

previously attributed to tumor-associated expression of cellular factors such as ATF3 (Mathew et al., 2020), galanin(Peters et al., 2005), and dynorphin, resulting in long-term phenotypic changes in sensory neurons. Alternation in neuronal discharge frequency and increased excitability in a greater proportion of wide dynamic range neurons from tumor induced mice (Khasabov et al., 2007) are additional evidence that points towards tumor induced phenotypic changes that occur in neurons innervating tumor tissue. Based on these studies, it is quite likely that even in the current study, the increase in DRG $(Ca^{2+})_i$ in tumor burdened rats is strongly associated with the development of primary (Kucharczyk et al., 2020) and distal hyperalgesia (Cain et al., 2001; de Clauser et al., 2020). Further, we found that ligand mediated activation of DOPr agonist, and TRPV1 blocker resulted in significant reduction in peak $(Ca^{2+})_i$ concentration in DRG's harvested from CIBP rats, although contributions from L-, N- and T-type Ca^{2+} channel blockers were limited.

While the DOPr agonist demonstrated good analgesia in CIBP animals, L-, N- calcium channel blockers, and TRPV1 antagonist failed to do so. Failure to achieve therapeutic dose, changes in receptor expression at the peripheral nerve terminals (Maqboul and Elsadek, 2018), or limited contribution of these blockers to antinociceptive activity (Julius, Basbaum, 2001; Mantyh et al., 2002) at the tumor site may be few reasons for this observation. In stark contrast, the T-type calcium channel blocker mibefradil, demonstrated poor reduction in peak $(Ca^{2+})_i$ concentration in DRG's harvested from CIBP rats, but robust reduction in primary hyperalgesia in CIBP animals. Our behavioural observations align well with previous studies that report considerable reduction in neuropathic and inflammatory pain with T-type blockers. However, the non-responsiveness of $(Ca^{2+})_i$ concentration in DRG neurons to mibefradil could be attributed to the fact that T-type channels modulates neuronal membrane excitability and contribute to neuronal firing by allowing only small changes in $(Ca^{2+})_i$, but their contribution to overt changes in $(Ca^{2+})_i$ concentration is minimal (Cain and Snutch, 2010; Shankarappa et al., 2011). It is also interesting to note that mibefradil shows dose-dependent attenuation of elicited pain at the local tumor site, but a similar dose-dependent effect is absent at the distal hindpaw site. The observed analgesic effect at the local site can be attributed to direct drug-receptor interaction since the drug solution is administered in the same location. However, the analgesia at the hindpaw is predominantly a central effect since the hindpaw sensory afferents arise from the lumbar spinal cord. It is plausible that the distal analgesia observed in the study may be due to drug leakage from the tumor area and the concentration difference may not elicit a measurable dose-response pattern.

Further, based on the mechanism of action of each of the drugs used, we had anticipated that the combination of DOPr agonist with the other drugs used in this study could have additive or synergistic effect on evoked Ca^{2+} response. However, at the concentration range tested, we did not observe any beneficial effect in terms of additivity or synergism. Previous studies have attributed low drug dosage ratio (Roca et al., 1996), and mutual interference of co-administered calcium antagonists at their binding sites for lack of additivity (Miranda and Paeile, 1990; Foucquier and Guedj, 2015), while others have suggested changes in channel conformation post receptor binding that could hinder further binding, thereby preventing drug synergy or additivity (Miranda and Paeile, 1990). The specific mechanisms for lack of additivity or

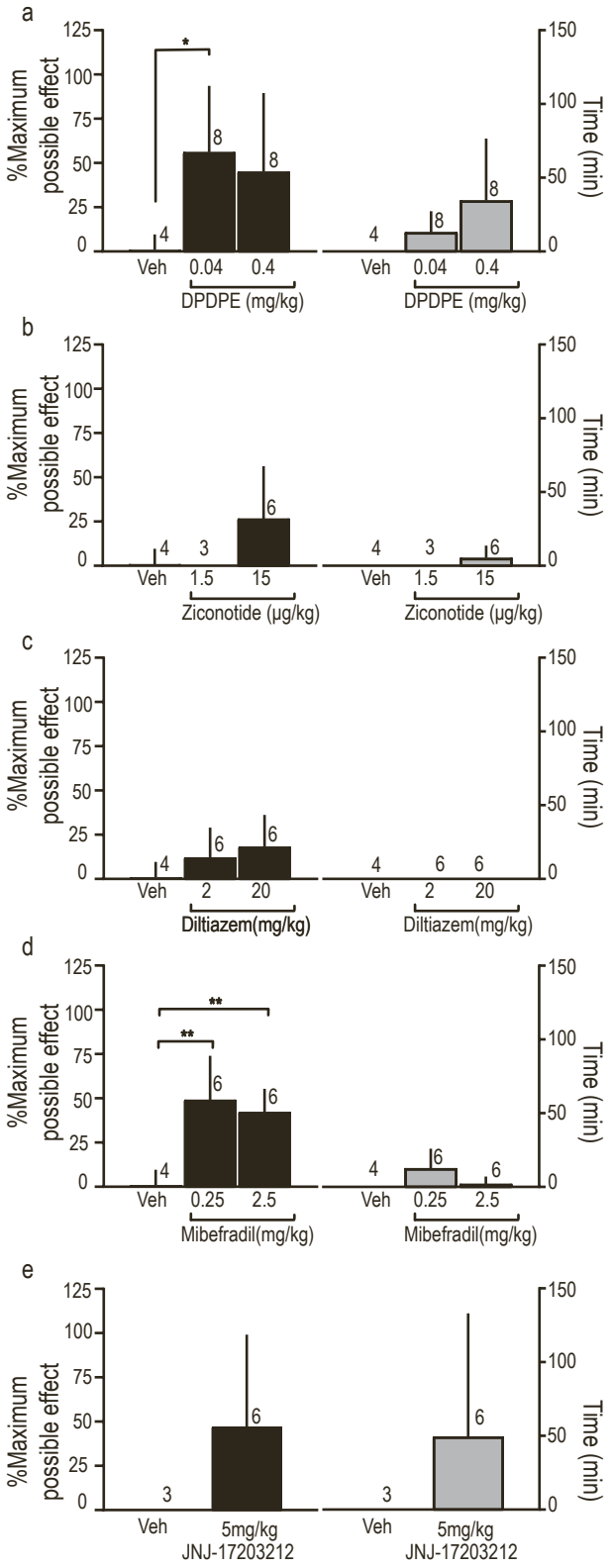

Fig. 6. Pain attenuation at distal site to tumor. The antinociceptive effect of analgesics administered via the peritumoral route was expressed as percent of maximum possible effect (MPE) (left Y axis, black bars). Duration of analgesia was calculated and quantified (right Y axis, grey bars). All behavioral responses were measured from the hind paw, distal to the tumor site, after application of a graded tactile stimulus to at the hind paw. Data shown as mean ± SD where number of rats tested per group is indicated on top of the bar graph. Statistical analysis was performed using one-way ANOVA with Dunnett's multiple comparison test compared to vehicle group, * indicates P value of < 0.05.

synergism were not tested in this study.

Mitigation of primary hyperalgesia by local injection of DOPr agonist was observed at a concentration of 0.4 mg/kg. Activation of DOPr is known to modulate cyclic AMP levels (cAMP) (Al-Hasani and Bruchas, 2011), and effect ERK1/2 (Eisinger and Ammer, 2008), p38 MAPK (Zhang et al., 1999), JNK, Akt(Kawaminami et al., 2022) and PLC pathways (Bie et al., 2010). In addition, DOPr activation has also been shown to increase G-protein coupled inward rectifying potassium channels (GIRK) (Shirasaki et al., 2004) and inhibit voltage-gated calcium channels (Wu et al., 2008) and thereby reduce neuronal excitability, and consequently dull the perception of pain (Quirion et al., 2020). Subcutaneous injection of the DOPr agonist, DPDPE, at a dose of 30–100 µg has been previously reported to produce naltrindole-sensitive attenuation (Baamonde et al., 2005) of tumor-induced thermal hyperalgesia in mice. Comparatively, administration of DOPr agonists via the intraperitoneal (Brainin-Mattos et al., 2006), intrathecal (Otis et al., 2011) or the intraplantar (Brigatte et al., 2013) routes require relatively lower doses to mitigate cancer induced pain. Curiously, we also observed that peritumoral administration of 0.4 mg/kg DPDPE and 0.25 mg/kg and 2.5 mg/kg of the T-type calcium channel antagonist attenuated hyperalgesia, both at the tumor site, as well as the distal site. Since intra-articular injection of the same drugs in the contralateral limb did not produce any discernible analgesia at the tumor site, it can be strongly surmised that the peri-tumoral mitigation of primary hyperalgesia is due to the local action of analgesics on tibial afferents and not primarily due to systemic leakage. However, it is inevitable that small amounts of systemic leakage of the drug is bound to occur in all forms of local injections, and this could be true in this study as well. Systemic leakage of DPDPE and the TRPV1 antagonist from the peritumoral site, could most likely produce mitigation of distal hyperalgesia via centrally located receptors at the level of spinal cord or brain. Though the analgesic effect of systemically administered N-, L- and T- type Ca^{2+} channel blockers on tumor-induced pain has been previously observed (Takasusuki and Yaksh, 2011), local administration of these drugs at the tumor site did not produce any analgesic effects. Further studies may be warranted with higher concentrations, though the risk of off-target effects will increase.

One of the limitation of this study has been the use of only one cancer model to assess the feasibility of local infiltration analgesia. Since different cancer types are unique in terms of their cellular components and microenvironment, it is quite possible that depending on the tumor type, neuronal phenotype within the tumor may be different, leading to the development of differential sensitivity to locally administered drugs. A systematic study looking into local analgesic responsivity in different tumor types would be warranted. Another limitation of this study is that it does not elaborately compare the difference in efficacy and dose-dependent toxicity between systemic and local infiltration analgesia. Although the primary goal of this study was not to compare the route of drug administration, information related to comparative efficacy and local tissue toxicity limits in future studies would be of help.

5. Conclusion

In conclusion, peritumoral administration of DOPr agonist and T-type calcium channel antagonists provide transient mitigation of pain at the tumor site in a model of bone cancer induced pain. The strategy of local infiltration analgesia around the tumor may not be practical for tumors that are inaccessible and those that may require major surgical access.

Funding

This work was supported in part, by grants from the Department of Biotechnology – BT/PR24515/MED/30/1926/2017 and from The Nanomission, Department of Science and Technology - DST/NM/NS-282/2019 (G), Government of India, to SS. PM received support from

CSIR-SRF fellowship (09/963(0046)−2K19EMR-1).

CRediT authorship contribution statement

Pallavi Madhusudanan: Methodology, Investigation, Analysis, Data curation, Visualization, Writing – original draft preparation Writing – review & editing. **Chinnu Jerard**: Investigation, Analysis, Data curation. **Gayathri Raju, Neeraj Katiyar**: Analysis. **Sahadev A. Shankarappa**: Conceptualization, Supervision, Project administration, Funding acquisition, Writing – review & editing, Formal analysis. All authors reviewed the manuscript.

Declaration of Competing Interest

The author(s) declare no competing interests.

Data availability

All raw data files used for analysis and quantification are available at https://doi.org/10.6084/m9.figshare.21187120.v3

Acknowledgements

The authors would like to acknowledge Mr. Arun, Mr. Vishnu, Mr. Sajith, Mr. Sunil, Mrs. Shanthini, Mrs. Sunitha, Dr. Sreekumar Kannoth, and Dr. A.K.K Unni for help involving animal experiments and DRG sample acquisition. We thank Dr. Siddaramaiah Gowda for technical assistance with micro-CT imaging. We also thank Mr. Arun and Ms. Aishwarya from Medhelix Diagnostics Pvt Ltd for technical assistance with tissue sections. We also thank Dr. Bipan Deb and Dr. Gaiti Hasan (NCBS, Bengaluru) for their valuable inputs in calcium imaging and calibrations. We also thank Mrs. Sumi E Mathew, Mr. Vignesh, Mr. Shivakumar for scientific discussions and valuable suggestions.

Appendix A. Supporting information

Supplementary data associated with this article can be found in the online version at doi:10.1016/j.neures.2023.06.006.

References

Afify, E.A., Andijani, N.M., 2017. Potentiation of morphine-induced antinociception by propranolol: The involvement of dopamine and GABA systems. Front. Pharmacol. 8 (NOV), 1–12. https://doi.org/10.3389/fphar.2017.00794.

Al-Hasani, R., Bruchas, M.R., 2011. Molecular mechanisms of opioid receptor-dependent signalling and behaviour. Anesthesiology 115 (6), 1363–1381. https://doi.org/10.1097/ALN.0b013e318238bba6.Molecular.

de Almeida, A.S., et al., 2021. Role of TRPA1 expressed in bone tissue and the antinociceptive effect of the TRPA1 antagonist repeated administration in a breast cancer pain model. Life Sci. 276 (Jul 1;276:119469) https://doi.org/10.1016/j.lfs.2021.119469.

Baamonde, A., et al., 2005. Effects of the local administration of selective μ-, δ-and κ-opioid receptor agonists on osteosarcoma-induced hyperalgesia. Naunyn-Schmiedeberg's Arch. Pharmacol. 372 (3), 213–219. https://doi.org/10.1007/s00210-005-0013-6.

Benyamin, R., et al., 2008. Opioid complications and side effects. Pain. Physician 11 (SPEC. ISS. 2), 105–120. https://doi.org/10.36076/ppj.2008/11/s105.

Bergström, J., et al., 2006. Opioid peptides and receptors in joint tissues: study in the rat. J. Orthop. Res. (June), 1121–1127. https://doi.org/10.1002/jor.20132.

Bie, B., et al., 2010. Nerve growth factor-regulated emergence of functional δ-opioid receptors. J. Neurosci. 30 (16), 5617–5628. https://doi.org/10.1523/JNEUROSCI.5296-09.2010.

Brainin-Mattos, J., et al., 2006. Cancer-related bone pain is attenuated by a systemically available δ-opioid receptor agonist. Pain 122 (1–2), 174–181. https://doi.org/10.1016/j.pain.2006.01.032.

Brigatte, P., et al., 2013. Peripheral kappa and delta opioid receptors are involved in the antinociceptive effect of crotalphine in a rat model of cancer pain. In: Pharmacology Biochemistry and Behavior, 109. Elsevier Inc,, pp. 1–7. https://doi.org/10.1016/j.pbb.2013.04.012.

Cahill, C.M., et al., 2003. Up-regulation and trafficking of δ opioid receptor in a model of chronic inflammation: Implications for pain control. Pain 101 (1–2), 199–208. https://doi.org/10.1016/S0304-3959(02)00333-0.

Cain, D.M., et al., 2001. Functional interactions between tumor and peripheral nerve: Changes in excitability and morphology of primary afferent fibers in a murine model of cancer pain. J. Neurosci. 21 (23), 9367–9376. https://doi.org/10.1523/jneurosci.21-23-09367.2001.

Cain, S.M., Snutch, T.P., 2010. Contributions of T-type calcium channel isoforms to neuronal firing. Channels 4 (6), 475–482. https://doi.org/10.4161/chan.4.6.14106.

de Clauser, L., et al., 2020. Sensitization of cutaneous primary afferents in bone cancer revealed by in vivo calcium imaging. Cancers 12 (12), 1–19. https://doi.org/10.3390/cancers12123491.

Colotta, F., et al., 2009. Cancer-related inflammation, the seventh hallmark of cancer: Links to genetic instability. Carcinogenesis 30 (7), 1073–1081. https://doi.org/10.1093/carcin/bgp127.

do Couto, N., et al., 2020. Measuring Intracellular Vesicle Density and Dispersion Using Fluorescence Microscopy and ImageJ/FIJI. Bio-Protoc. 10 (15), 1–11. https://doi.org/10.21769/bioprotoc.3703.

van den Beuken-van Everdingen, M.H.J., et al., 2007. Prevalence of pain in patients with cancer: A systematic review of the past 40 years. Ann. Oncol. 18 (9), 1437–1449. https://doi.org/10.1093/annonc/mdm056.

Dushyanthen, S., Cossigny, D.A.F., Quan, G.M.Y., 2013. The osteoblastic and osteoclastic interactions in spinal metastases secondary to prostate cancer. Cancer Growth Metastas-.-. 6, 61–80. https://doi.org/10.4137/CGM.s12769.

Eisinger, D.A., Ammer, H., 2008. δ-Opioid receptors activate ERK/MAP kinase via integrin-stimulated receptor tyrosine kinases. In: Cellular Signalling, 20. Elsevier Inc,, pp. 2324–2331. https://doi.org/10.1016/j.cellsig.2008.09.002.

Falk, S., Dickenson, A.H., 2014. Pain and nociception: Mechanisms of cancer-induced bone pain. J. Clin. Oncol. 32 (16), 1647–1654. https://doi.org/10.1200/JCO.2013.51.7219.

Foucquier, J., Guedj, M., 2015. Analysis of drug combinations: current methodological landscape. Pharmacol. Res. Perspect. 3 (3) https://doi.org/10.1002/prp2.149.

Fuchs, A., et al., 2007. Contribution of Calcium Channel Subtypes to the Intracellular Calcium Signal in Sensory Neurons: The Effect of Injury. Anesthesiology 107 (1), 117–127 doi: 10.1097/01.anes.0000267511.21864.93. Contribution.

Ghilardi, J.R., et al., 2005. Selective Blockade of the Capsaicin Receptor TRPV1 Attenuates Bone Cancer Pain. J. Neurosci. 25 (12), 3126–3131. https://doi.org/10.1523/JNEUROSCI.3815-04.2005.

Giray, B., et al., 2018. Comparison of nerve fiber density between patients with uterine leiomyoma with and without pain: A prospective clinical study. Geburtshilfe und Frauenheilkd. 78 (4), 407–411. https://doi.org/10.1055/a-0591-1751.

Iwasaki, T., et al., 2019. Reduction of intrapancreatic neural density in cancer tissue predicts poorer outcome in pancreatic ductal carcinoma. Cancer Sci. 110 (4), 1491–1502. https://doi.org/10.1111/cas.13975.

Jerard, C. et al. (2023) Secretome mediated interactions between sensory neurons and breast cancer cells., International journal of cancer. United States. doi: 10.1002/ijc.34529.

Jochmann, E., et al., 2015. Antigen-induced arthritis in rats is associated with increased growth-associated protein 43-positive intraepidermal nerve fibres remote from the joint. *Arthritis Res. Ther.* Arthritis Res. Ther. 17 (1), 1–15. https://doi.org/10.1186/s13075-015-0818-8.

Julius, D., Basbaum, I., A., 2001. Molecular mechanisms of nociception. Nature 413, 203–210. https://doi.org/10.1038/35093019.

Katiyar, N., et al., 2021. Neuronal delivery of nanoparticles via nerve fibres in the skin. In: Scientific Reports, 11. Nature Publishing Group UK,, pp. 1–13. https://doi.org/10.1038/s41598-021-81995-x.

Kawaminami, A., et al., 2022. Selective δ-Opioid Receptor Agonist, KNT-127, Facilitates Contextual Fear Extinction via Infralimbic Cortex and Amygdala in Mice. Front. Behav. Neurosci. 16 (February), 1–14. https://doi.org/10.3389/fnbeh.2022.808232.

Khasabov, S.G., et al., 2007. Tumor-evoked hyperalgesia and sensitization of nociceptive dorsal horn neurons in a murine model of cancer pain. Brain Res 1180, 7–19. https://doi.org/10.1016/j.brainres.2007.08.075.

Khasabova, I.A., et al., 2007. Chemical Interactions between Fibrosarcoma Cancer Cells and Sensory Neurons Contribute to Cancer Pain. J. Neurosci. 27 (38), 10289–10298. https://doi.org/10.1523/JNEUROSCI.2851-07.2007.

Kucharczyk, M.W., et al., 2020. The impact of bone cancer on the peripheral encoding of mechanical pressure stimuli. Pain 161 (8), 1894–1905. https://doi.org/10.1097/j.pain.0000000000001880.

Latremoliere, A., Woolf, C.J., 2009. Central Sensitization: A Generator of Pain Hypersensitivity by Central Neural Plasticity. J. Pain. 10 (19), 895–926. https://doi.org/10.1016/j.jpain.2009.06.012.Central.

Lautner, M.A., et al., 2011. In vitro sarcoma cells release a lipophilic substance that activates the pain transduction system via TRPV1. Ann. Surg. Oncol. 18 (3), 866–871. https://doi.org/10.1245/s10434-010-1328-1.

Li, Y., et al., 2015. The cancer chemotherapeutic paclitaxel increases human and rodent sensory neuron responses to TRPV1 by activation of TLR4. J. Neurosci. 35 (39), 13487–13500. https://doi.org/10.1523/JNEUROSCI.1956-15.2015.

Mantyh, P.W., et al., 2002. Molecular mechanisms of cancer pain. Nat. Rev. Cancer 2 (3), 201–209. https://doi.org/10.1038/nrc747.

Maqboul, A., Elsadek, B., 2018. Expression profiles of TRPV1, TRPV4, TLR4 and ERK1/2 in the dorsal root ganglionic neurons of a cancer-induced neuropathy rat model. PeerJ 2018 (4). https://doi.org/10.7717/peerj.4622.

Mathew, S.E., Madhusudanan, P., Shankarappa, S.A., 2020. Effect of peritumoral bupivacaine on primary and distal hyperalgesia in cancer-induced bone pain. J. Pain. Res. 13, 1305–1313. https://doi.org/10.2147/JPR.S250198.

Matsuo, K., et al., 2019. Innervation of the tibial epiphysis through the intercondylar foramen. In: Bone, 120. Elsevier Inc,, pp. 297–304. https://doi.org/10.1016/j.bone.2018.11.007.

Menéndez, L., et al., 2003. Peripheral opioids act as analgesics in bone cancer pain in mice. NeuroReport 14 (6), 867–869. https://doi.org/10.1097/00001756-200305060-00018.

Miranda, H.F., Paeile, C., 1990. Interactions between analgesics and calcium channel blockers. Gen. Pharmacol. 21 (2), 171–174. https://doi.org/10.1016/0306-3623(90)90896-T.

Niiyama, Y., et al., 2009. SB366791, a TRPV1 antagonist, potentiates analgesic effects of systemic morphine in a murine model of bone cancer pain. Br. J. Anaesth. 102 (2), 251–258. https://doi.org/10.1093/bja/aen347.

Otis, V., Sarret, P., Gendron, L., 2011. Spinal activation of delta opioid receptors alleviates cancer-related bone pain. Neuroscience 183 (819), 221–229. https://doi.org/10.1016/j.neuroscience.2011.03.052.

Peters, C.M., et al., 2005. Tumor-induced injury of primary afferent sensory nerve fibers in bone cancer pain. Exp. Neurol. 193 (1), 85–100. https://doi.org/10.1016/j.expneurol.2004.11.028.

Quirion, B., et al., 2020. The Delta-Opioid Receptor; a Target for the Treatment of Pain. Front. Mol. Neurosci. 13 (May), 1–11. https://doi.org/10.3389/fnmol.2020.00052.

Roca, G., et al., 1996. Nimodipine fails to enhance the analgesic effect of slow release morphine in the early phases of cancer pain treatment. Pain 68 (2–3), 239–243. https://doi.org/10.1016/S0304-3959(96)03186-7.

Sabino, M.A.C., et al., 2003. Different tumors in bone each give rise to a distinct pattern of skeletal destruction, bone cancer-related pain behaviors and neurochemical changes in the central nervous system. Int. J. Cancer 104 (5), 550–558. https://doi.org/10.1002/ijc.10999.

Sandkühler, J., 2009. Models and mechanisms of hyperalgesia and allodynia. Physiol. Rev. 89 (2), 707–758. https://doi.org/10.1152/physrev.00025.2008.

Schmidt, B.L., et al., 2010. Mechanisms of cancer pain. Mol. Interv. 10 (3), 164–178. https://doi.org/10.1124/mi.10.3.7.

Shankarappa, S.A., Piedras-Renteria, E.S., Stubbs Jr., E.B., 2011. Forced-exercise delays neuropathic pain in experimental diabetes: effects on voltage-activated calcium channels. J. Neurochem. 118 (2), 224–236. https://doi.org/10.1111/j.1471-4159.2011.07302.x.

Shirasaki, T., et al., 2004. δ-Opioid receptor antagonists inhibit GIRK channel currents in acutely dissociated brainstem neurons of rat. Brain Res. 1006 (2), 190–197. https://doi.org/10.1016/j.brainres.2004.02.004.

Silverman, D.A., et al., 2021. Cancer-associated neurogenesis and nerve-cancer crosstalk. Cancer Res 81 (6), 1431–1440. https://doi.org/10.1158/0008-5472.CAN-20-2793.

Sliepen, S.H.J., 2021. Bone Cancer Pain, Mechanism and Treatment. In: Amarasekera, H. (Ed.), Recent Advances in Bone Tumours and Osteoarthritis. Rijeka: IntechOpen. https://doi.org/10.5772/intechopen.95910.

Takasusuki, T., Yaksh, T.L., 2011. Regulation of spinal substance P release by intrathecal calcium channel blockade. Anesthesiology 115 (1), 153–164. https://doi.org/10.1097/ALN.0b013e31821950c2.

Urch, C., 2004. The pathophysiology of cancer-induced bone pain: Current understanding. Palliat. Med. 18 (4), 267–274. https://doi.org/10.1191/0269216304pm887ra.

Urch, C.E., Donovan-Rodriguez, T., Dickenson, A.H., 2003. Alterations in dorsal horn neurones in a rat model of cancer-induced bone pain. Pain 106 (3), 347–356. https://doi.org/10.1016/j.pain.2003.08.002.

Vuong, S., et al., 2016. Inadequate pain management in cancer patients attending an outpatient palliative radiotherapy clinic. Support. Care Cancer 24 (2), 887–892. https://doi.org/10.1007/s00520-015-2858-7.

Wu, Z.Z., Chen, S.R., Pan, H.L., 2008. Distinct inhibition of voltage-activated Ca2+ channels by δ-opioid agonists in dorsal root ganglion neurons devoid of functional T-type Ca2+ currents. Neuroscience 153 (4), 1256–1267. https://doi.org/10.1016/j.neuroscience.2008.03.031.

Zhang, Z., et al., 1999. Endogenous δ-opioid and ORL1 receptors couple to phosphorylation and activation of p38 MAPK in NG108-15 cells and this is regulated by protein kinase A and protein kinase C. J. Neurochem. 73 (4), 1502–1509. https://doi.org/10.1046/j.1471-4159.1999.0731502.x.

Zhao, C.M., et al., 2014. Denervation suppresses gastric tumorigenesis. Sci. Transl. Med. 6 (250) https://doi.org/10.1126/scitranslmed.3009569.

Zheng, X.Q., et al., 2022. Neurophysiological mechanisms of cancer-induced bone pain. *J. Adv. Res.* Authors 35 (xxxx), 117–127. https://doi.org/10.1016/j.jare.2021.06.006.